WCNS schemes and some recent developments

Yaming Chen[1*] and Xiaogang Deng[1,2]

*Correspondence:
chenym-08@163.com

[1] College of Aerospace
Science and Engineering,
National University of Defense
Technology, Changsha 410073,
China
[2] Chinese Academy of Military
Science, Beijing 100071, China

Abstract

Weighted compact nonlinear schemes (WCNS) are a family of nonlinear shock capturing schemes that are suitable for solving problems with discontinuous solutions. The schemes are based on grids staggered by flux points and solution points, resulting in algorithms with the nonlinear interpolation step independent of the difference step. Thus, only linear difference operators are needed, such that geometric conservation law can be preserved easily, resulting in the preservation of freestream condition. In recent years, these schemes have attracted a lot of attention in the community of computational fluid dynamics. This paper intends to give a brief review of the basic algorithms of these schemes and present some related recent developments.

Keywords: WCNS, Conservation law, Shock capturing, Boundary closure, Geometric conservation law

1 Introduction

With the fast growth of computational capability, high-order methods play a more and more important role in the field of computational fluid dynamics. High-order schemes, usually referred to schemes with convergence rates higher than second-order, admit better resolution properties than their lower order counterparts. More importantly, high-order schemes may produce more accurate results than low-order schemes in terms of using the same computational cost. In the past three decades, great progress has been achieved for high-order schemes. Some representative schemes are widely used, such as weighted essentially non-oscillatory (WENO) schemes [1–3], weighted compact nonlinear schemes (WCNS) [4], discontinuous Galerkin schemes [5–7], spectral difference schemes [8–10], flux reconstruction schemes [11, 12], and so on.

WCNS schemes are a family of high-order schemes that are suitable for solving problems with discontinuous solutions. These schemes are originally developed for addressing shock-capturing problems of compact linear schemes [13]. Although dissipation can be introduced to improve the shock capturing capability of compact linear schemes [14], oscillations are difficult to be removed for strong shocks. Therefore, nonlinear schemes are often needed. In [15, 16], based on grids staggered by flux

points and solution points, compact nonlinear schemes were developed by employing the idea of ENO schemes for the interpolation step. Later on, the idea of WENO schemes was introduced further to construct WCNS schemes [4, 17]. Since then, WCNS schemes were further developed and widely used in applications [18]. Some benchmark examples were presented in [19] to demonstrate the efficiency of WCNS schemes. They were used in Reynolds-averaged Navier-Stokes (RANS) simulations [20–26], large eddy simulations (LES) [27–32], hybrid RANS/LES simulations [33, 34], and even direct numerical simulations (DNS) [35]. Some important phenomena were also investigated by applying these schemes. The areas include boundary layer transition [36–40], acoustic wave [41–44], vortices [45], interaction between shock wave and vortex [46, 47], detonation [48–50], body-wake interactions [51], Mach reflection [52], elastic-plastic deformation [53], multi-component compressible flows [54], magneto-hydrodynamics [55], and so on.

Compared with WENO schemes, WCNS schemes have some advantages, mainly lying in the flexibility of the choice of numerical fluxes and the convenience of preserving geometric conservation law. In this paper, we provide a brief review of WCNS schemes, aiming at introducing some basic ideas of the algorithms and presenting some recent developments. The rest of this paper is arranged as follows. In Section 2, the basic algorithm of WCNS schemes is given. In Section 3, conservative boundary closures are discussed. In Section 4, geometric conservation law that arises from coordinate transform is presented. To preserve this law numerically, a symmetric conservative metric method (SCMM) is also introduced. Finally, concluding remarks are given in Section 5.

2 Algorithm of WCNS schemes

To describe WCNS schemes, let us consider the one-dimensional conservation law

$$u_t + f(u)_x = 0, \tag{1}$$

where $u = u(x,t)$ denotes the conservative quantity and $f(u)$ is the flux. As illustrated in Fig. 1, the spatial interval $[a, b]$ is divided into N subintervals by flux points

$$x_{j+1/2} = a + jh, \quad 0 \le j \le N, \tag{2}$$

where $h = (b-a)/N$ stands for the length of the interval. The solution points, denoted by x_j, are placed at the center of the subintervals $[x_{j-1/2}, x_{j+1/2}]$, i.e.,

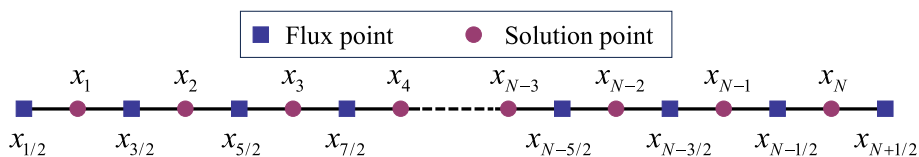$$x_j = (x_{j-1/2} + x_{j+1/2})/2, \quad 1 \le j \le N. \tag{3}$$

Fig. 1 Illustration of the grid staggered by flux points and solution points

2.1 Basic procedure

At time t, suppose the values of u at solution points x_j are known, denoted by u_j. Then the spatial discretization algorithm of WCNS schemes can be summarized as the following three steps:

  (i) Apply interpolation schemes to obtain the left and right values at flux points $x_{j+1/2}$, denoted by $u^L_{j+1/2}$ and $u^R_{j+1/2}$, respectively.
  (ii) Compute the numerical flux $f_{j+1/2} = \hat{f}\left(u^L_{j+1/2}, u^R_{j+1/2}\right)$, where $\hat{f}$ denotes some approximate Riemann solvers.
  (iii) Employ difference schemes to calculate the flux derivatives at solution points x_j, denoted by f'_j.

After spatial discretization, we obtain a system of ordinary differential equations

$$\frac{du_j}{dt} + f'_j = 0, \tag{4}$$

which can be solved by some time-marching schemes, such as the explicit Runge-Kutta scheme [56], the two-stage fourth-order scheme [57], and some other implicit schemes [58, 59]. It shall be mentioned that one can also perform interpolation for the flux directly as done in [60]. However, in that case the nonlinearity is performed for the flux, leading to the difficulty in preserving geometric conservation law, which is very important for applications to complex configurations.

2.2 Interpolation schemes

For the interpolation step, many interpolation schemes can be applied. For smooth solutions, linear interpolation schemes can be applied, such as explicit upwind interpolation schemes [61], compact upwind linear interpolation schemes [13], dissipative compact linear interpolation schemes [62, 63], and so on.

  Here, we introduce a fifth-order interpolation scheme [4] for the left values, while the right values can be obtained according to the symmetry property of the grids. As illustrated in Fig. 2, to get the left values $u^L_{j+1/2}$ at flux points $x_{j+1/2}$, the following explicit upwind fifth-order interpolation scheme can be derived, i.e.,

$$u^L_{j+1/2} = \frac{3}{128}u_{j-2} - \frac{5}{32}u_{j-1} + \frac{45}{64}u_j + \frac{15}{32}u_{j+1} - \frac{5}{128}u_{j+2}, \tag{5}$$

where the coefficients can be obtained by using the method of Lagrangian interpolation. However, this scheme is not suitable for the case with discontinuous solutions. To address this problem, one may first decompose the fifth-order scheme (5) as
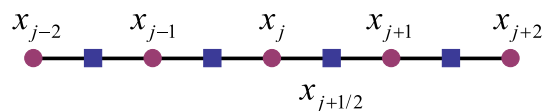

Fig. 2 Illustration of the stencil used for the fifth-order interpolation scheme (5)

$$u_{j+1/2}^L = \sum_{k=0}^{2} \gamma_k u_{j+1/2}^{(k)}, \tag{6}$$

where $u_{j+1/2}^{(k)}$ are third-order interpolation schemes with different stencils, expressed as

$$u_{j+1/2}^{(0)} = \frac{3}{8}u_{j-2} - \frac{5}{4}u_{j-1} + \frac{15}{8}u_j, \tag{7}$$

$$u_{j+1/2}^{(1)} = -\frac{1}{8}u_{j-1} + \frac{3}{4}u_j + \frac{3}{8}u_{j+1}, \tag{8}$$

$$u_{j+1/2}^{(2)} = \frac{3}{8}u_j + \frac{3}{4}u_{j+1} - \frac{1}{8}u_{j+2}, \tag{9}$$

and γ_k are linear optimal weights with values

$$\gamma_0 = \frac{1}{16}, \quad \gamma_1 = \frac{5}{8}, \quad \gamma_2 = \frac{5}{16}. \tag{10}$$

Then, following the recipe of WENO schemes [3] we introduce nonlinear weights defined by

$$\omega_k = \frac{\alpha_k}{\alpha_0 + \alpha_1 + \alpha_2}, \tag{11}$$

where

$$\alpha_k = \frac{\gamma_k}{(\beta_k + \varepsilon)^2}. \tag{12}$$

Here, the small parameter ε is set to be 10^{-6} to avoid the denominator becoming zero, and β_k are smoothness indicators of the interpolation schemes applied to compute $u_{j+1/2}^{(k)}$, defined by

$$\beta_0 = (u_{j-2} - 2u_{j-1} + u_j)^2 + \frac{1}{4}(u_{j-2} - 4u_{j-1} + 3u_j)^2, \tag{13}$$

$$\beta_1 = (u_{j-1} - 2u_j + u_{j+1})^2 + \frac{1}{4}(u_{j-1} - u_{j+1})^2, \tag{14}$$

$$\beta_2 = (u_j - 2u_{j+1} + u_{j+2})^2 + \frac{1}{4}(3u_j - 4u_{j+1} + u_{j+2})^2. \tag{15}$$

Finally, we obtain the fifth-order shock capturing interpolation scheme

$$u_{j+1/2}^L = \sum_{k=0}^{2} \omega_k u_{j+1/2}^{(k)}. \tag{16}$$

However, it was pointed out in [64] that the scheme (16) based on the nonlinear weights defined by Eqs. (11) and (12) may degenerate to third-order at critical points. To address
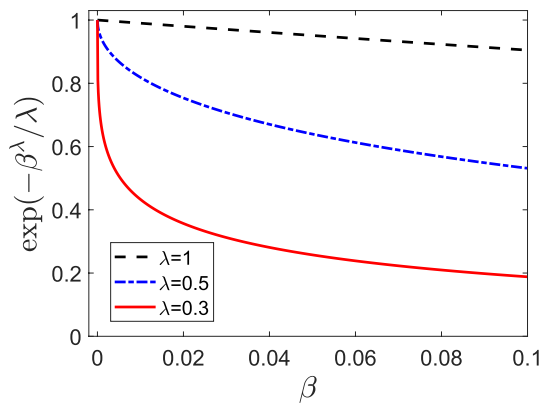
Fig. 3 The exponential function involved in Eq. (17)

this issue, one can implement the idea of improving the performance of WENO schemes for the nonlinear interpolation step of WCNS schemes. In particular, we present here a recent work [65] such that the optimal fifth-order convergence rate can be achieved for any smooth solutions, i.e., regardless of the order of critical points. The scheme can still be written in the form of Eq. (16), where ω_k are still given by Eq. (11), but with α_k defined by

$$\alpha_k = \gamma_k \exp(-\beta_k^\lambda/\lambda). \tag{17}$$

Here, β_k are still given by Eqs. (13)-(15), and λ is a parameter defined by

$$\lambda = \max\left(e^{-3\theta}, 10^{-6}\right), \quad \theta = \frac{\tau}{(\beta_{\min} + \varepsilon)^{0.8}}, \tag{18}$$

where

$$\tau = |\beta_2 - \beta_0|, \quad \beta_{\min} = \min_{k=0,1,2} \beta_k, \quad \varepsilon = 10^{-40}. \tag{19}$$

It can be seen from Fig. 3 that α_k are more sensitive to the values of β_k for smaller value of λ. For smooth solutions, the definition of λ (18) satisfies the condition

$$\lim_{h \to 0} \lambda = 1. \tag{20}$$

Since the smoothness indicators defined by Eqs. (13)-(15) obey the relations $\beta_k = \mathcal{O}(h^2)$, we have

$$\alpha_k = \gamma_k + \mathcal{O}(h^2). \tag{21}$$

This condition ensures that the corresponding scheme (16) is fifth-order, regardless of the order of critical points.

There are some other methods for improving the performance of the nonlinear interpolation schemes. For example, low-dissipation WCNS schemes were constructed in [66–71]. In [72–74], compact nonlinear interpolation schemes were developed to improve the resolution of WCNS schemes. The ideas of targeted ENO schemes and multi-resolution WENO schemes were introduced for the interpolation step of WCNS schemes in [75] and [76, 77], respectively. A parameter-free ε-adaptive algorithm was also proposed in [78, 79] to improve the performance of WCNS schemes.

2.3 Difference schemes

By using interpolation schemes, we can get the left and right values at flux points $x_{j+1/2}$. Then various approximate Riemann solvers [80–82] can be applied to compute the numerical fluxes $f_{j+1/2}$ at flux points $x_{j+1/2}$. It shall be mentioned that both flux vector splitting and flux difference splitting methods are applicable here for WCNS schemes, while only flux vector splitting methods can be applied for reconstruction-based WENO schemes. In [83–86], the effect of flux evaluation methods for WCNS schemes was investigated in details. Here we pay attention to difference schemes.

It was shown in [87, 88] that the resolution of WCNS schemes is dominated by the compactness of the interpolation step, while it is less related to the difference step. Therefore, the difference scheme is usually chosen to be an explicit one for the purpose of efficiency. For instance, the sixth-order explicit central difference scheme presented in [87, 89] reads as

$$f_j' = \frac{75}{64}\frac{f_{j+1/2} - f_{j-1/2}}{h} - \frac{25}{128}\frac{f_{j+3/2} - f_{j-3/2}}{3h} + \frac{3}{128}\frac{f_{j+5/2} - f_{j-5/2}}{5h}. \tag{22}$$

For the reason of robustness, some other hybrid difference schemes involving both the fluxes at flux points and solution points can also be used. For example, the sixth-order scheme presented in [90] can be written as

$$\begin{aligned} f_j' = {}& \alpha\frac{f_{j+1/2} - f_{j-1/2}}{h} + \frac{192 - 175\alpha}{256}\frac{f_{j+1} - f_{j-1}}{h} + \frac{35\alpha - 48}{320}\frac{f_{j+2} - f_{j-2}}{h} \\ & + \frac{64 - 45\alpha}{3840}\frac{f_{j+3} - f_{j-3}}{h}, \end{aligned} \tag{23}$$

where $\alpha \geq 0$ is a parameter that can be tuned to control its dissipation property. The sixth-order difference scheme implemented in [91] is expressed as

$$f_j' = \frac{3}{2}\frac{f_{j+1/2} - f_{j-1/2}}{h} - \frac{3}{10}\frac{f_{j+1} - f_{j-1}}{h} + \frac{1}{30}\frac{f_{j+3/2} - f_{j-3/2}}{h}. \tag{24}$$

It was shown that WCNS schemes can benefit from linear difference operators in terms of preserving geometric conservation law [92, 93]. It shall also be mentioned that alternative WENO schemes were proposed in [94], where the WENO reconstruction is employed for the variable rather than the flux. Thus, linear difference operators can be applied directly. It shall be mentioned that the alternative WENO schemes are closely related to WCNS schemes, as pointed out in [95, 96]. Since it is not easy to find the original conference paper [95] for the derivation in details, we present the demonstration of the relation in Appendix A.

3 Conservative boundary closures

Compared to interior schemes of WCNS schemes, boundary closures are seldom considered theoretically. Although some concerns have been mentioned in previous works, the stability issue has not been clearly investigated. By using the result of Gustafsson [97], the order of boundary closures should be at most one order lower than that of the interior for first-order hyperbolic conservation laws. Otherwise, the global convergence rate cannot be equal to the order of the interior. For Cartesian grids, the inverse Lax-Wendroff method [98–100] may be applied to derive the boundary closures. However, this method is difficult for applications to practical problems. In most cases, we may need curvilinear grids and apply biased schemes near boundary.

For WCNS schemes, conservative boundary closures were derived based on global conservation in [61]. Some applications can also be found in [101, 102]. The derivation is based on the difference scheme consisting of only flux points, like the sixth-order difference scheme (5). For a more general case, we introduce here the method used in [61] and consider the $2r$th-order difference scheme

$$f_j' = \sum_{k=1}^{r} \alpha_k \frac{f_{j+k-1/2} - f_{j-k+1/2}}{(2k-1)h}, \quad r \le j \le N - r + 1, \tag{25}$$

where the coefficients α_k can be determined according to the order condition. For instance, one can apply the method of Lagrangian interpolation to get the values of α_k as tabulated in Table 1 for $2 \le r \le 6$.

To mimic the global conservation property of the one-dimensional conservation law (1), i.e.,

$$\frac{d}{dt} \int_a^b u\,dx = f(u(a,t)) - f(u(b,t)), \tag{26}$$

we first rewrite the interior difference scheme (25) into a conservative form

$$f_j' = \frac{\widetilde{f}_{j+1/2} - \widetilde{f}_{j-1/2}}{h}, \tag{27}$$

where

$$\widetilde{f}_{j+1/2} = \sum_{k=1}^{r} \frac{\alpha_k}{2k-1} \sum_{l=j-k+1}^{j+k-1} f_{l+1/2}. \tag{28}$$

Table 1 The values of α_k in Eq. (25) for $2 \le r \le 6$

r	α_1	α_2	α_3	α_4	α_5	α_6
2	$\frac{9}{8}$	$-\frac{1}{8}$				
3	$\frac{75}{64}$	$-\frac{25}{128}$	$\frac{3}{128}$			
4	$\frac{1225}{1024}$	$-\frac{245}{1024}$	$\frac{49}{1024}$	$-\frac{5}{1024}$		
5	$\frac{19845}{16384}$	$-\frac{2205}{8192}$	$\frac{567}{8192}$	$-\frac{405}{32768}$	$\frac{35}{32768}$	
6	$\frac{160083}{131072}$	$-\frac{38115}{131072}$	$\frac{22869}{262144}$	$-\frac{5445}{262144}$	$\frac{847}{262144}$	$-\frac{63}{262144}$

Then we define the interior operator as

$$\mathcal{I}[f] = \sum_{j=r}^{N-r+1} f_j' = \frac{\widetilde{f}_{N-r+3/2} - \widetilde{f}_{r-1/2}}{h}. \tag{29}$$

Finally, we introduce the left and right boundary operators, written respectively as

$$\mathcal{L}[f] = \frac{\widetilde{f}_{r-1/2} - f_{1/2}}{h} \tag{30}$$

and

$$\mathcal{R}[f] = \frac{f_{N+1/2} - \widetilde{f}_{N-r+3/2}}{h}, \tag{31}$$

such that the following global conservation property holds

$$(\mathcal{L}[f] + \mathcal{I}[f] + \mathcal{R}[f])h = f_{N+1/2} - f_{1/2}. \tag{32}$$

Now what we need to do is just to decompose the boundary operators as the sum of the difference schemes at solution points near boundary. Due to the symmetry property of the grid, we only have to consider the case for the left. It was shown in [61] that

$$\mathcal{L}[f] = \sum_{j=1}^{r-1} f'(x_j) + \mathcal{O}(h), \tag{33}$$

which means that there must be as least a near boundary difference scheme with only first order of accuracy if we require $\mathcal{L}[f] = \sum_{j=1}^{r-1} f_j'$. To address this issue, we modified Eq. (33) to be

$$\mathcal{L}[f] = \sum_{j=1}^{r-1} \omega_j f'(x_j^*) + \mathcal{O}(h^{2r-2}), \tag{34}$$

where the $2r-2$ unknowns, ω_j and x_j^*, are determined by the conditions of the accuracy. Here, the new introduced solution points x_j^* are nonuniformly distributed, which are called conservative solution points. The detailed values of ω_j and x_j^* can be found in [61]; see Eqs. (32)-(36) therein. That is to say, we replace the solution points near boundary with the conservative points and consider so-called semi-uniform grids, where the flux points are still uniformly distributed, as illustrated in Fig. 4.

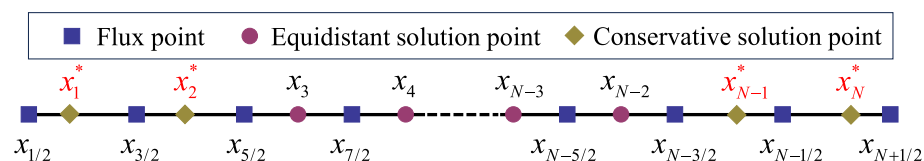To determine the conservative difference schemes near boundary, we first require that

Fig. 4 Illustration of the semi-uniform grid for the fifth-order WCNS scheme, where the two solution points near each boundary are replaced with the conservative solution points

$$\mathcal{L}[f] = \sum_{j=1}^{r-1} \omega_j f_j'. \tag{35}$$

Then we set the schemes f_j' to be $(2r-2)$th-order, determined by the following stencils

$$f_j' = \frac{1}{h} \sum_{k=1}^{2r-1} a_{j,k} f_{k-1/2}, \tag{36}$$

where the coefficients $a_{j,k}$ can be determined conveniently by using the method of Lagrangian interpolation. For the right-hand side, the boundary closures for the difference scheme can be obtained symmetrically.

For the interpolation step, we just need to apply interpolation schemes with biased stencils. Then we can construct boundary closures that are time stable up to eleventh order of global accuracy. For problems with discontinuous solutions near boundary, nonlinear shock-capturing boundary interpolation schemes were proposed recently in [103]. It was shown that the shock-capturing issue near boundary can be resolved well by using the idea of multi-resolution interpolation and the technique of tuning parameter in the smoothness indicators.

4 Geometric conservation law and SCMM method

For practical applications, it often necessitates to apply curvilinear grids. In that case, we shall consider conservation law in curvilinear coordinates. Since the pioneering work [104], some problems related to geometric conservation law have been studied by many researchers [92, 93, 105–109]. According to [110], the geometric conservation law can be classified as surface conservation law and volume conservation law. For static curvilinear grids, which is the case considered in this paper, the volume conservation law is satisfied automatically. Thus, we only need to consider the surface conservation law.

4.1 Surface conservation law

To describe the definition of the surface conservation law, let us consider the three-dimensional conservation law, written as

$$U_t + F_x + G_y + H_z = 0, \tag{37}$$

where U denotes the conservative quantity, and F, G and H are fluxes in x, y and z directions, respectively. In curvilinear coordinates (ξ, η, ζ) [111], Eq. (37) can be expressed as

$$(JU)_t + \left(\mathcal{F} \cdot \mathbf{S}^{(\xi)} \right)_\xi + \left(\mathcal{F} \cdot \mathbf{S}^{(\eta)} \right)_\eta + \left(\mathcal{F} \cdot \mathbf{S}^{(\zeta)} \right)_\zeta = 0, \tag{38}$$

where $\mathcal{F} = (F, G, H)$ is the tensor of the fluxes, and the Jacobian term J is defined as

$$J = \mathbf{r}_\xi \cdot (\mathbf{r}_\eta \times \mathbf{r}_\zeta), \tag{39}$$

and the surface vectors $\mathbf{S}^{(\xi)}$, $\mathbf{S}^{(\eta)}$ and $\mathbf{S}^{(\zeta)}$ are determined by

$$\mathbf{S}^{(\xi)} = \mathbf{r}_\eta \times \mathbf{r}_\zeta, \quad \mathbf{S}^{(\eta)} = \mathbf{r}_\zeta \times \mathbf{r}_\xi, \quad \mathbf{S}^{(\zeta)} = \mathbf{r}_\xi \times \mathbf{r}_\eta \tag{40}$$

with $\mathbf{r} = (x, y, z)^T$. It is straightforward to check that the following relation holds, i.e.,

$$\left(\mathbf{S}^{(\xi)}\right)_{\xi} + \left(\mathbf{S}^{(\eta)}\right)_{\eta} + \left(\mathbf{S}^{(\zeta)}\right)_{\zeta} = 0, \tag{41}$$

which is the so-called surface conservation law.

4.2 SCMM method

In the context of discretization space, the surface conservation law (41) may not hold exactly, leading to geometric induced errors in the solution. It was shown that preserving the surface conservation law discretely is very important for high-order finite different schemes [106].

For low-order algorithms [104, 112], some techniques can be made to satisfy the surface conservation law discretely. For high-order finite different schemes, according to the knowledge of the authors, the most satisfied way so far is to apply the SCMM method with linear difference operators. This method is a further development of the conservative metric method (CMM) proposed in [92]. The CMM method can maintain the freestream property of the original conservation law and also improve the behavior of WCNS schemes for applications to curvilinear coordinates [18]. However, the CMM method does not admit appropriate geometric meaning that is similar with finite volume methods. To address this issue, the SCMM method was proposed in [93].

The SCMM method is based on the symmetric conservative form of the Jacobian (39) and the surface vectors (40), where the Jacobian is written as

$$J = \frac{1}{3}\left[\left(\mathbf{r}\cdot\mathbf{S}^{(\xi)}\right)_{\xi} + \left(\mathbf{r}\cdot\mathbf{S}^{(\eta)}\right)_{\eta} + \left(\mathbf{r}\cdot\mathbf{S}^{(\zeta)}\right)_{\zeta}\right], \tag{42}$$

and the surface vectors are expressed as

$$\mathbf{S}^{(\xi)} = \frac{1}{2}\left[(\mathbf{r}\times\mathbf{r}_{\zeta})_{\eta} + (\mathbf{r}_{\eta}\times\mathbf{r})_{\zeta}\right], \tag{43}$$

$$\mathbf{S}^{(\eta)} = \frac{1}{2}[(\mathbf{r}\times\mathbf{r}_{\xi})_{\zeta} + (\mathbf{r}_{\zeta}\times\mathbf{r})_{\xi}], \tag{44}$$

$$\mathbf{S}^{(\zeta)} = \frac{1}{2}[(\mathbf{r}\times\mathbf{r}_{\eta})_{\xi} + (\mathbf{r}_{\xi}\times\mathbf{r})_{\eta}]. \tag{45}$$

For the SCMM method, linear difference operators are applied to discretize the metric derivatives. The discretization of the Jacobian term is denoted as

$$\begin{aligned}
J_{j,k,l} = &\frac{1}{3}\delta_{\xi}^{1}\left\{\mathbf{r}\cdot\frac{1}{2}\left[\delta_{\eta}^{2}\left(\mathbf{r}\times\delta_{\zeta}^{3}\mathbf{r}\right) + \delta_{\zeta}^{2}\left(\delta_{\eta}^{3}\mathbf{r}\times\mathbf{r}\right)\right]\right\}_{j,k,l} \\
&+ \frac{1}{3}\delta_{\eta}^{1}\left\{\mathbf{r}\cdot\frac{1}{2}\left[\delta_{\zeta}^{2}\left(\mathbf{r}\times\delta_{\xi}^{3}\mathbf{r}\right) + \delta_{\xi}^{2}\left(\delta_{\zeta}^{3}\mathbf{r}\times\mathbf{r}\right)\right]\right\}_{j,k,l} \\
&+ \frac{1}{3}\delta_{\zeta}^{1}\left\{\mathbf{r}\cdot\frac{1}{2}\left[\delta_{\xi}^{2}\left(\mathbf{r}\times\delta_{\eta}^{3}\mathbf{r}\right) + \delta_{\eta}^{2}\left(\delta_{\xi}^{3}\mathbf{r}\times\mathbf{r}\right)\right]\right\}_{j,k,l},
\end{aligned} \tag{46}$$

where δ_ξ^n, δ_η^n and δ_ζ^n ($n = 1, 2, 3$) denote the linear difference operators for ξ, η and ζ directions, respectively. Here the superscripts are counted from outside to inside of the brackets.

The spatial term of Eq. (38) has a similar form to the Jacobian (42), and its discretized form can be expressed as

$$
\begin{aligned}
SDT_{j,k,l} = \frac{1}{3}\delta_\xi^1 &\left\{ \mathcal{F} \cdot \frac{1}{2}\left[\delta_\eta^2\left(\mathbf{r} \times \delta_\zeta^3\mathbf{r}\right) + \delta_\zeta^2\left(\delta_\eta^3\mathbf{r} \times \mathbf{r}\right)\right]\right\}_{j,k,l} \\
+ \frac{1}{3}\delta_\eta^1 &\left\{ \mathcal{F} \cdot \frac{1}{2}\left[\delta_\zeta^2\left(\mathbf{r} \times \delta_\xi^3\mathbf{r}\right) + \delta_\xi^2\left(\delta_\zeta^3\mathbf{r} \times \mathbf{r}\right)\right]\right\}_{j,k,l} \\
+ \frac{1}{3}\delta_\zeta^1 &\left\{ \mathcal{F} \cdot \frac{1}{2}\left[\delta_\xi^2\left(\mathbf{r} \times \delta_\eta^3\mathbf{r}\right) + \delta_\eta^2\left(\delta_\xi^3\mathbf{r} \times \mathbf{r}\right)\right]\right\}_{j,k,l}.
\end{aligned}
\tag{47}
$$

For freestream flow, U is constant, so is $\mathcal{F}$. In that case, if the linear difference operators satisfy the condition

$$
\delta_\xi^1 = \delta_\xi^2, \quad \delta_\eta^1 = \delta_\eta^2, \quad \delta_\zeta^1 = \delta_\zeta^2,
\tag{48}
$$

then it is easy to observe from Eq. (47) that

$$
SDT_{j,k,l} = 0.
\tag{49}
$$

Therefore, the semi-discretized form of Eq. (38) becomes

$$
\frac{d}{dt}(JU)_{j,k,l} = 0.
\tag{50}
$$

Since static grids are considered here, the Jacobian is independent of time. Thus, we know from Eq. (50) that $U_{j,k,l}$ is constant, indicating that the freestream condition is preserved exactly. Actually, the condition (48) also ensures that the surface conservation law (41) is maintained discretely. However, if we intend to have some geometric meanings of the Jacobian, it is better to further require that

$$
\delta_\xi^1 = \delta_\xi^2 = \delta_\xi^3, \quad \delta_\eta^1 = \delta_\eta^2 = \delta_\eta^3, \quad \delta_\zeta^1 = \delta_\zeta^2 = \delta_\zeta^3,
\tag{51}
$$

which is the condition of the SCMM method. In this case, the discretized value $J_{j,k,l}$ (46) represents a weighted sum of some volumes consisting of grid points in the physical space [113, 114].

5 Conclusions

In this paper, we have summarized some main algorithms of WCNS schemes and presented some related recent developments. The schemes are based on grids staggered by flux points and solution points. Thus, the spatial discretization is divided into the interpolation step and the difference step. This setup has benefit in the flexibility of choosing numerical fluxes. In addition, the nonlinear procedure is applied only to the interpolation step but not the difference step. Thus, the geometric conservation law can be preserved exactly in a discrete setting, providing that the introduced SCMM method is applied. We have also introduced the so-called conservative boundary closures for the

difference step, such that the scheme is globally conservative and also time stable, with the global convergent rates as the same as the interior.

In future, some aspects of WCNS schemes are worth studying further, mainly lying in the improvement of their robustness, accuracy and resolution. To improve the robustness of the schemes for practical applications, one should address the issue of positivity preserving [115–117]. So far, how to preserve the positivity property and the geometric conservation law on curvilinear grids at the same time is still an open problem. Although a fifth-order WCNS scheme with unconditionally optimal convergence rate is available [65], the extension to other orders of accuracy shall be addressed. In addition, for a given grid the actual truncation error of a scheme is determined by its resolution. Thus, to improve the resolution property of WCNS schemes [118] deserves a further study as well.

Appendix A: Relation between WCNS and alternative WENO schemes

The alternative WENO schemes [94] for the one-dimensional conservation law (1) can be written as

$$\frac{du_j}{dt} + \frac{\hat{f}_{j+1/2} - \hat{f}_{j-1/2}}{h} = 0, \tag{52}$$

where

$$\hat{f}_{j+1/2} = f_{j+1/2} - \frac{1}{24}h^2 f_{xx}|_{j+1/2} + \frac{7}{5760}h^4 f_{xxxx}|_{j+1/2} + \mathcal{O}(h^6). \tag{53}$$

If we drop the truncation error and evaluate the derivatives in the above equation by the following central difference schemes,

$$f_{xx}|_{j+1/2} = \frac{1}{h^2}\left[-\frac{17}{24}(f_j + f_{j+1}) + \frac{13}{16}(f_{j-1} + f_{j+2}) - \frac{5}{48}(f_{j-2} + f_{j+3})\right], \tag{54}$$

$$f_{xxxx}|_{j+1/2} = \frac{1}{h^4}\left[(f_j + f_{j+1}) - \frac{3}{2}(f_{j-1} + f_{j+2}) + \frac{1}{2}(f_{j-2} + f_{j+3})\right], \tag{55}$$

then we have

$$\hat{f}_{j+1/2} = f_{j+1/2} + \frac{59}{1920}(f_j + f_{j+1}) - \frac{137}{3840}(f_{j-1} + f_{j+2}) + \frac{19}{3840}(f_{j-2} + f_{j+3}). \tag{56}$$

In this case, the spatial discretization term $(\hat{f}_{j+1/2} - \hat{f}_{j-1/2})/h$ in Eq. (52) is equal to that of the WCNS scheme (4) with the difference scheme

$$f'_j = \frac{f_{j+1/2} - f_{j-1/2}}{h} + \frac{17}{256}\frac{f_{j+1} - f_{j-1}}{h} - \frac{13}{320}\frac{f_{j+2} - f_{j-2}}{h} + \frac{19}{3840}\frac{f_{j+3} - f_{j-3}}{h}, \tag{57}$$

which is exactly the hybrid sixth-order difference scheme (23) with $\alpha = 1$.

Availability of data and materials
The data used in this paper are available from the corresponding author on reasonable request.

Declarations

Competing interests
The authors declare that they have no competing interests.

References
1. Harten A, Engquist B, Osher S et al (1987) Uniformly high order accurate essentially non-oscillatory schemes, III. J Comput Phys 71:231–303. https://doi.org/10.1016/0021-9991(87)90031-3
2. Liu XD, Osher S, Chan T (1994) Weigted essentially non-oscillatory schemes. J Comput Phys 115:200–212. https://doi.org/10.1006/jcph.1994.1187
3. Jiang GS, Shu CW (1996) Efficient implementation of weighted ENO schemes. J Comput Phys 126:202–228. https://doi.org/10.1006/jcph.1996.0130
4. Deng X, Zhang H (2000) Developing high-order weighted compact nonlinear schemes. J Comput Phys 165:22–44. https://doi.org/10.1006/jcph.2000.6594
5. Reed WH, Hill TR (1973) Triangular mesh methods for the neutron transport equation. Los Alamos Scientific Laboratory Report, LA-UR-73-479. https://www.osti.gov/biblio/4491151
6. Cockburn B, Shu CW (1989) TVB Runge-Kutta local projection discontinuous Galerkin finite element method for conservation laws II: General framework. Math Comput 52:411–435. https://doi.org/10.1090/S0025-5718-1989-0983311-4
7. Bassi F, Rebay S (1997) A high-order accurate discontinuous finite element method for the numerical solution of the compressible Navier-Stokes equations. J Comput Phys 131:267–279. https://doi.org/10.1006/jcph.1996.5572
8. Kopriva DA, Kolias JH (1996) A conservative staggered-grid Chebyshev multidomain method for compressible flows. J Comput Phys 125:244–261. https://doi.org/10.1006/jcph.1996.0091
9. Liu Y, Vinokur M, Wang ZJ (2006) Spectral difference method for unstructured grids I: Basic formulation. J Comput Phys 216:780–801. https://doi.org/10.1016/j.jcp.2006.01.024
10. Wang ZJ, Liu Y, May G et al (2006) Spectral difference method for unstructured grids II: Extension to the Euler equations. J Sci Comput 32:45–71. https://doi.org/10.1007/s10915-006-9113-9
11. Huynh HT (2007) A flux reconstruction approach to high-order schemes including discontinuous Galerkin methods. In: 18th AIAA computational fluid dynamics conference. AIAA, Miami, p 2007–4079. https://doi.org/10.2514/6.2007-4079
12. Huynh HT (2009) A reconstruction approach to high-order schemes including discontinuous Galerkin for diffusion. In: 47th AIAA aerospace sciences meeting including the new horizons forum and aerospace exposition. AIAA, Orlando, p 2009–403. https://doi.org/10.2514/6.2009-403
13. Lele SK (1992) Compact finite difference schemes with spectral-like resolution. J Comput Phys 103:16–42. https://doi.org/10.1016/0021-9991(92)90324-R
14. Deng X, Maekawa H, Shen C (1996) A class of high-order dissipative compact schemes. In: 27th fluid dynamics conferences. AIAA, New Orleans, p 96–1972. https://doi.org/10.2514/6.1996-1972
15. Deng X, Maekawa H (1996) A uniform fourth-order compact scheme for discontinuities capturing. In: 27th fluid dynamics conferences. AIAA, New Orleans, p 96–1974. https://doi.org/10.2514/6.1996-1974
16. Deng X, Maekawa H (1997) Compact high-order accurate nonlinear schemes. J Comput Phys 130:77–91. https://doi.org/10.1006/jcph.1996.5553
17. Deng X, Mao M (1997) Weighted compact high-order nonlinear schemes for the Euler equations. In: 13th computational fluid dynamics conference. AIAA, Snowmass Village, p 97–1941. https://doi.org/10.2514/6.1997-1941
18. Deng X, Mao M, Tu G et al (2012) High-order and high accurate CFD methods and their applications for complex grid problems. Commun Comput Phys 11:1081–1102. https://doi.org/10.4208/cicp.100510.150511s
19. Wang S, Deng X, Wang G et al (2016) Efficiency benchmarking of seventh-order tri-diagonal weighted compact nonlinear scheme on curvilinear mesh. Int J Comput Fluid Dyn 30:469–488. https://doi.org/10.1080/10618562.2016.1248425
20. Tu G, Deng X, Mao M (2012) Assessment of two turbulence models and some compressibility corrections for hypersonic compression corners by high-order difference schemes. Chin J Aeronaut 25:25–32. https://doi.org/10.1016/S1000-9361(11)60358-0

21. Tu G, Deng X, Mao M (2013) Validation of a RANS transition model using a high-order weighted compact nonlinear scheme. Sci China-Phys Mech Astron 56:805–811. https://doi.org/10.1007/S11433-013-5037-1

22. Wang S, Dong Y, Deng X et al (2018) High-order simulation of aeronautical separated flows with a Reynold stress model. J Aircr 55:1177–1190. https://doi.org/10.2514/1.C034628

23. Wang S, Deng X, Wang G et al (2020) Blending the eddy-viscosity and Reynolds-stress models using uniform high-order discretization. AIAA J 58:5361–5378. https://doi.org/10.2514/1.j059180

24. Fu X, Wang S, Deng X (2022) Assessment of alternative scale-providing variables in a Reynolds-stress model using high-order methods. Acta Mech Sin 38:322151. https://doi.org/10.1007/s10409-022-22151-x

25. Fu X, Deng X, Wang S et al (2022) High-order discretization of the Reynolds stress model with an ϵ_β-adaptive algorith. Acta Mech Sin 38:321357. https://doi.org/10.1007/s10409-021-09084-x

26. Wang S, Fu X, Deng X (2022) Higher-order aerodynamic numerical simulations in compressible RANS framework with inverse-ω scale variable. Aerosp Sci Technol 131:107971. https://doi.org/10.1016/j.ast.2022.107971

27. Ishiko K, Ohnishi N, Ueno K et al (2009) Implicit large eddy simulation of two-dimensional homogeneous turbulence using weighted compact nonlinear scheme. J Fluids Engin 131:061401. https://doi.org/10.1115/1.3077141

28. Matsukawa Y (2011) Implicit large eddy simulation of a supersonic flat-plate boundary layer flow by weighted compact nonlinear scheme. Int J Comput Fluid Dyn 25:47–57. https://doi.org/10.1080/10618562.2011.555334

29. Tatsukawa T, Nonomura T, Oyama A et al (2016) Multi-objective aeroacoustic design exploration of launch-pad flame deflector using large-eddy simulation. J Spacecr Rockets 53:751–758. https://doi.org/10.2514/1.A33420

30. Zebiri B, Piquet A, Hadjadj A et al (2020) Shock-induced flow separation in an overexpanded supersonic planar nozzle. AIAA J 58:2122–2131. https://doi.org/10.2514/1.j058705

31. Zebiri B, Piquet A, Hadjadj A (2021) On the use of a two-layer model for large-eddy simulations of supersonic boundary layers with separation. Int J Heat Fluid Flow 90:108821. https://doi.org/10.1016/J.IJHEATFLUIDFLOW.2021.108821

32. Koga K, Kajishima T (2023) Semi-explicit large eddy simulation in non-reacting air/gas fuel jet flows. J Adv Simulat Sci Eng 10:1–20. https://doi.org/10.15748/jasse.10.1

33. Yang Y, Wang H, Sun M et al (2019) Numerical investigation of transverse jet in supersonic crossflow using a high-order nonlinear filter scheme. Acta Astronaut 154:74–81. https://doi.org/10.1016/j.actaastro.2018.10.006

34. Browne OMF, Housman JA, Kenway GKW et al (2023) Numerical investigation of $c_{L,max}$ prediction on the NASA high-lift common research model. AIAA J 61:1639–1658. https://doi.org/10.2514/1.j062508

35. Hiejima T (2020) Helicity effects on inviscid instability in Batchelor vortices. J Fluid Mech 897:A37. https://doi.org/10.1017/jfm.2020.388

36. Zhao Y, Liu W, Xu D et al (2016) A combined experimental and numerical investigation of roughness induced supersonic boundary layer transition. Acta Astronaut 118:199–209. https://doi.org/10.1016/J.ACTAASTRO.2015.10.008

37. Zhou Y, Zhao YF, Xu D et al (2016) Numerical investigation of hypersonic flat-plate boundary layer transition mechanism induced by different roughness shapes. Acta Astronaut 127:209–218. https://doi.org/10.1016/J.ACTAASTRO.2016.05.027

38. Zhou Y, Liu W, Chai Z et al (2017) Numerical simulation of wavy surface effect on the stability of a hypersonic boundary layer. Acta Astronaut 140:485–496. https://doi.org/10.1016/J.ACTAASTRO.2017.08.018

39. Wang S, Ge M, Deng X et al (2019) Blending of algebraic transition model and subgrid model for separated transitional flows. AIAA J 57:4684–4697. https://doi.org/10.2514/1.J058313

40. Liu S, Yuan X, Liu Z et al (2021) Design and transition characteristics of a standard model for hypersonic boundary layer transition research. Acta Mech Sin 37:1637–1647. https://doi.org/10.1007/s10409-021-01136-5

41. Fujii K, Nonomura T, Tsutsumi S (2010) Toward accurate simulation and analysis of strong acoustic wave phenomena—A review from the experience of our study on rocket problems. Int J Numer Meth Fluids 64:1412–1432. https://doi.org/10.1002/fld.2446

42. Nonomura T, Goto Y, Fujii K (2011) Aeroacoustic waves generated from a supersonic jet impinging on an inclined flat plate. Int J Aeroacoustics 10:401–425. https://doi.org/10.1260/1475-472X.10.4.401

43. Nonomura T, Fujii K (2011) Overexpansion effects on characteristics of Mach waves from a supersonic cold jet. AIAA J 49:2282–2294. https://doi.org/10.2514/1.J051054

44. Nonomura T, Honda H, Nagata Y et al (2016) Plate-angle effects on acoustic waves from supersonic jets impinging on inclined plates. AIAA J 54:816–827. https://doi.org/10.2514/1.J054152

45. Hiejima T (2014) Spatial evolution of supersonic streamwise vortices. Phys Fluids 26:074102. https://doi.org/10.1063/1.4886097

46. Zuo Z, Maekawa H (2014) Computational study of the interaction between a shock and a near-wall vortex using a weighted compact nonlinear scheme. Fluid Dyn Res 46:015508. https://doi.org/10.1088/0169-5983/46/1/015508

47. Hiejima T (2014) Criterion for vortex breakdown on shock wave and streamwise vortex interactions. Phys Rev E 89:053017. https://doi.org/10.1103/PHYSREVE.89.053017

48. Iida R, Asahara M, Hayashi AK et al (2014) Implementation of a robust weighted compact nonlinear scheme for modeling of hydrogen/air detonation. Combust Sci Technol 186:1736–1757. https://doi.org/10.1080/00102202.2014.935646

49. Niibo T, Morii Y, Ashahara M et al (2016) Numerical study on direct initiation of cylindrical detonation in H_2/O_2 mixtures: effect of higher-order schemes on detonation propagation. Combust Sci Technol 188:2044–2059. https://doi.org/10.1080/00102202.2016.1215109

50. Takeshima N, Ozawa K, Tsuboi N et al (2020) Numerical simulations on propane/oxygen detonation in a narrow channel using a detailed chemical mechanism: formation and detailed structure of irregular cells. Shock Waves 30:809–824. https://doi.org/10.1007/s00193-020-00978-5

51. Jiang Y, Mao M, Deng X et al (2015) Numerical investigation on body-wake flow interaction over rod-airfoil configuration. J Fluid Mech 779:1–35. https://doi.org/10.1017/jfm.2015.419

52. Qin Z, Shi A, Dowell EH et al (2022) Analytical model of strong Mach reflection. AIAA J 60:5187–5202. https://doi.org/10.2514/1.J061701

53. Ghaisas NS, Subramaniam A, Lele SK (2018) A unified high-order Eulerian method for continuum simulations of fluid flow and of elastic-plastic deformations in solids. J Comput Phys 371:452–482. https://doi.org/10.1016/j.jcp.2018.05.035

54. Koga K, Kajishima T (2022) Low dissipative finite difference hybrid scheme by discontinuity sensor of detecting shock and material interface in multi-component compressible flows. J Comput Phys 448:110757. https://doi.org/10.1016/j.jcp.2021.110757

55. Minoshima T, Miyoshi T, Matsumoto Y (2019) A high-order weighted finite difference scheme with a multistate approximate Riemann solver for divergence-free magnetohydrodynamic simulations. Astrophys J Suppl S 242:14. https://doi.org/10.3847/1538-4365/ab1a36

56. Shu CW, Osher S (1988) Efficient implementation of essentially non-oscillatory shock-capturing schemes. J Comput Phys 77:439–471. https://doi.org/10.1016/0021-9991(88)90177-5

57. He Z, Gao F, Tian B et al (2020) Implementation of finite difference weighted compact nonlinear schemes with the two-stage fourth-order accurate temporal discretization. Commun Comput Phys 27:1470–1484. https://doi.org/10.4208/cicp.OA-2019-0029

58. Li D, Xu C, Cheng B et al (2017) Performance modeling and optimization of parallel LU-SGS on many-core processors for 3D high-order CFD simulations. J Supercomput 73:2506–2524. https://doi.org/10.1007/s11227-016-1943-0

59. Jiang Y, Zhou S, Zhang X et al (2022) High order all-speed semi-implicit weighted compact nonlinear scheme for the isentropic Navier-Stokes equations. J Comput Appl Math 411:114272. https://doi.org/10.1016/j.cam.2022.114272

60. Zhang S, Jiang S, Shu CW (2008) Development of nonlinear weighted compact schemes with increasingly higher order accuracy. J Comput Phys 227:7294–7321. https://doi.org/10.1016/j.jcp.2008.04.012

61. Deng X, Chen Y (2018) A novel strategy for deriving high-order stable boundary closures based on global conservation, I: Basic formulas. J Comput Phys 372:80–106. https://doi.org/10.1016/j.jcp.2018.06.012

62. Deng X, Jiang Y, Mao M et al (2013) Developing hybrid cell-edge and cell-node dissipative compact scheme for complex geometry flows. Sci China Technol Sci 56:2361–2369. https://doi.org/10.1007/S11431-013-5339-6

63. Deng X, Jiang Y, Mao M et al (2015) A family of hybrid cell-edge and cell-node dissipative compact schemes satisfying geometric conservation law. Comput Fluids 116:29–45. https://doi.org/10.1016/j.compfluid.2015.04.015

64. Henrick AK, Aslam TD, Powers JM (2005) Mapped weighted essentially non-oscillatory schemes: Achieving optimal order near critical points. J Comput Phys 207:542–567. https://doi.org/10.1016/j.jcp.2005.01.023

65. Chen Y, Deng X (2023) Nonlinear weights for shock capturing schemes with unconditionally optimal high order. J Comput Phys 478:111978. https://doi.org/10.1016/j.jcp.2023.111978

66. Wong ML, Lele SK (2017) High-order localized dissipation weighted compact nonlinear scheme for shock and interface-capturing in compressible flows. J Comput Phys 339:179–209. https://doi.org/10.1016/j.jcp.2017.03.008

67. Kamiya T, Asahara M, Nonomura T (2017) Application of central differencing and low-dissipation weights in a weighted compact nonlinear scheme. Int J Numer Meth Fluids 84:152–180. https://doi.org/10.1002/fld.4343

68. Jin Y, Liao F, Cai J (2018) Optimized low-dissipation and low-dispersion schemes for compressible flows. J Comput Phys 371:820–849. https://doi.org/10.1016/j.jcp.2018.05.049

69. Zhao G, Sun M, Xie S et al (2018) Numerical dissipation control in an adaptive WCNS with a new smoothness indicator. Appl Math Comput 330:239–253. https://doi.org/10.1016/j.amc.2018.01.019

70. Zhang H, Zhang F, Liu J et al (2020) A simple extended compact nonlinear scheme with adaptive dissipation control. Commun Nonlinear Sci Numer Simul 84:105191. https://doi.org/10.1016/j.cnsns.2020.105191

71. Hong Z, Ye Z, Ye K (2021) An optimised five-point-stencil weighted compact nonlinear scheme for hyperbolic conservation laws. Int J Comput Fluid Dyn 35:179–196. https://doi.org/10.1080/10618562.2021.1906419

72. Subramaniam A, Wong ML, Lele SK (2019) A high-order weighted compact high resolution scheme with boundary closures for compressible turbulent flows with shocks. J Comput Phys 397:108822. https://doi.org/10.1016/j.jcp.2019.07.021

73. Jin Y, Liao F, Cai J (2020) Compact schemes for multiscale flows with cell-centered finite difference method. J Sci Comput 85:17. https://doi.org/10.1007/s10915-020-01314-w

74. Ma Y, Yan Z, Liu H et al (2022) Improved weighted compact nonlinear scheme for implicit large eddy simulations. Comput Fluids 240:105412. https://doi.org/10.1016/j.compfluid.2022.105412

75. Zhang H, Zhang F, Xu C (2018) Towards optimal high-order compact schemes for simulating compressible flows. Appl Math Comput 355:221–237. https://doi.org/10.1016/j.amc.2019.03.001

76. Zhang H, Wang G, Zhang F (2020) A multi-resolution weighted compact nonlinear scheme for hyperbolic conservation laws. Inter J Comput Fluid Dynam 34:187–203. https://doi.org/10.1080/10618562.2020.1722807

77. Wang Z, Zhu J, Wang CW et al (2023) An efficient hybrid multi-resolution WCNS scheme for solving compressible flows. J Comput Phys 477:111877. https://doi.org/10.1016/j.jcp.2022.111877

78. Zheng S, Deng X, Wang D et al (2019) A parameter-free ϵ-adaptive algorithm for improving weighted compact nonlinear schemes. Int J Numer Meth Fluids 90:247–266. https://doi.org/10.1002/fld.4719

79. Huang Z, Zheng S, Wang D et al (2022) A new ϵ-adaptive algorithm for improving weighted compact nonlinear scheme with applications. Aerospace 9:369. https://doi.org/10.3390/aerospace9070369

80. Roe PL (1981) Approximate Riemann solvers, parameter vectors, and difference schemes. J Comput Phys 43:357–372. https://doi.org/10.1016/0021-9991(81)90128-5

81. van Leer B (1979) Towards the ultimate conservative difference scheme. V. A second-order sequel to Godunov's method. J Comput Phys 32:101–136. https://doi.org/10.1016/0021-9991(79)90145-1

82. Steger JL, Warming RF (1981) Flux vector splitting of the inviscid gasdynamic equations with applications to finite difference methods. J Comput Phys 40:263–293. https://doi.org/10.1016/0021-9991(81)90210-2

83. Tu G, Zhao X, Mao M et al (2014) Evaluation of Euler fluxes by a high-order CFD scheme: shock instability. Int J Comput Fluid Dyn 28:171–186. https://doi.org/10.1080/10618562.2014.911847

84. Tu G, Chen J, Mao M et al (2016) On the splitting methods of inviscid fluxes for implementing high-order weighted compact nonlinear schemes. Appl Math Mech 37:1324–1344. https://doi.org/10.21656/1000-0887.370518

85. Wang D, Deng X, Wang G et al (2016) Developing a hybrid flux function suitable for hypersonic flow simulation with high-order methods. Int J Numer Meth Fluids 81:309–327. https://doi.org/10.1002/fld.4186

86. Kamiya T, Asahara M, Nonomura T (2020) Effect of flux evaluation methods on the resolution and robustness of the two-step finite-difference WENO scheme. Numer Math Theor Meth Appl 13:1068–1097. https://doi.org/10.4208/nmtma.OA-2019-0033

87. Deng X, Liu X, Mao M et al (2005) Investigation on weighted compact fifth-order nonlinear scheme and applications to complex flow. In: 17th AIAA computational fluid dynamics conference. AIAA, Toronto, p 2005–5246. https://doi.org/10.2514/6.2005-5246

88. Nonomura T, Fujii K (2009) Effects of difference scheme type in high-order weighted compact nonlinear schemes. J Comput Phys 228:3533–3539. https://doi.org/10.1016/j.jcp.2009.02.018

89. Liu X, Deng X, Mao M (2007) High-order behaviors of weighted compact fifth-order nonlinear schemes. AIAA J 45:2093–2097. https://doi.org/10.2514/1.23797

90. Deng X, Mao M, Jiang Y et al (2011) New high-order hybrid cell-edge and cell-node weighted compact nonlinear schemes. In: 20th AIAA computational fluid dynamics conference. AIAA, Honolulu, p 2011–3857. https://doi.org/10.2514/6.2011-3857

91. Nonomura T, Fujii K (2013) Robust explicit formulation of weighted compact nonlinear scheme. Comput Fluids 85:8–18. https://doi.org/10.1016/j.compfluid.2012.09.001

92. Deng X, Mao M, Tu G et al (2011) Geometric conservation law and applications to high-order finite difference schemes with stationary grids. J Comput Phys 230:1100–1115. https://doi.org/10.1016/j.jcp.2010.10.028

93. Deng X, Min Y, Mao M et al (2013) Further studies on geometric conservation law and applications to high-order finite difference schemes with stationary grids. J Comput Phys 239:90–111. https://doi.org/10.1016/j.jcp.2012.12.002

94. Jiang Y, Shu CW, Zhang M (2013) An alternative formulation of finite difference weighted ENO schemes with Lax-Wendroff time discretization for conservation laws. SIAM J Sci Comput 35:A1137–A1160. https://doi.org/10.1137/120889885

95. Asahara M, Nonomura T, Fujii K et al (2013) Comparison of resolution and robustness with TS-WENO schemes. In: Proceedings of the 27th Computational Fluid Dynamics Symposium, vol C03-4 (in Japanese)

96. Nonomura T, Terakado D, Abe Y et al (2015) A new technique for freestream preservation of finite-difference WENO on curvilinear grid. Comput Fluids 107:242–255. https://doi.org/10.1016/J.COMPFLUID.2014.09.025

97. Gustafsson B (1975) The convergence rate for difference approximations to mixed initial boundary value problems. Math Comp 29:396–406. https://doi.org/10.1090/S0025-5718-1975-0386296-7

98. Tan S, Shu CW (2010) Inverse Lax-Wendroff procedure for numerical boundary conditions of conservation laws. J Comput Phys 229:8144–8166. https://doi.org/10.1016/j.jcp.2010.07.014

99. Tan S, Wang C, Shu CW et al (2012) Efficient implementation of high order inverse Lax-Wendroff boundary treatment for conservation laws. J Comput Phys 231:2510–2527. https://doi.org/10.1016/j.jcp.2011.11.037

100. Hao T, Chen Y, Tang L et al (2023) A third-order weighted nonlinear scheme for hyperbolic conservation laws with inverse Lax-Wendroff boundary treatment. Appl Math Comput 441:127697. https://doi.org/10.1016/j.amc.2022.127697

101. Deng X, Chen Y, Xu D et al (2017) A novel boundary treatment method for global seventh-order dissipative compact finite-difference scheme. In: 23rd AIAA computational fluid dynamics conference. AIAA, Denver, p 2017–4497. https://doi.org/10.2514/6.2017-4497

102. Chen Y, Deng X (2019) A stable dissipative compact finite difference scheme with global accuracy of ninth order. Comput Fluids 185:13–21. https://doi.org/10.1016/j.compfluid.2019.04.002

103. Qin J, Chen Y, Lin Y et al (2023) On construction of shock-capturing boundary closures for high-order finite difference method. Comput Fluids 255:105818. https://doi.org/10.1016/j.compfluid.2023.105818

104. Thomas PD, Lombard CK (1979) Geometric conservation law and its application to flow computations on moving grids. AIAA J 17:1030–1037. https://doi.org/10.2514/3.61273

105. Vinokur M (1989) An analysis of finite-difference and finite-volume formulations of conservation laws. J Comput Phys 81:1–52. https://doi.org/10.1016/0021-9991(89)90063-6

106. Visbal MR, Gaitonde DV (2002) On the use of higher-order finite-difference schemes on curvilinear and deforming meshes. J Comput Phys 181:155–185. https://doi.org/10.1006/jcph.2002.7117

107. Nonomura T, Iizuka N, Fujii K (2010) Freestream and vortex preservation properties of high-order WENO and WCNS on curvilinear grids. Comput Fluids 39:197–214. https://doi.org/10.1016/j.compfluid.2009.08.005

108. Abe Y, Iizuka N, Nonomura T et al (2013) Conservative metric evaluation for high-order finite difference schemes with the GCL identities on moving and deforming grids. J Comput Phys 232:14–21. https://doi.org/10.1016/j.jcp.2012.08.031

109. Abe Y, Nonomura T, Iizuka N et al (2014) Geometric interpretations and spatial symmetry property of metrics in the conservative form for high-order finite-difference schemes on moving and deforming grids. J Comput Phys 260:163–203. https://doi.org/10.1016/j.jcp.2013.12.019

110. Zhang H, Reggio M, Trepanier JY et al (1993) Discrete form of the GCL for moving meshes and its implementation in CFD schemes. Comput Fluids 22:9–23. https://doi.org/10.4208/aamm.OA-2017-0098

111. Sjögreen B, Yee H, Vinokur M (2014) On high order finite-difference metric discretizations satisfying GCL on moving and deforming grids. J Comput Phys 265:211–220. https://doi.org/10.1016/j.jcp.2014.01.045

112. Pulliam TH, Steger JL (1980) Implicit finite-difference simulations of three-dimensional compressible flow. AIAA J 18:159–167. https://doi.org/10.2514/3.50745

113. Deng X, Zhu H, Min Y et al (2014) Symmetric conservative metric method: a link between high order finite-difference and finite-volume schemes for flow computations around complex geometries. In: 8th international conference on computational fluid dynamics. Chengdu

114. Deng X, Zhu H, Min Y et al (2020) High-order finite difference schemes based on symmetric conservative metric method: decomposition, geometric meaning and connection with finite volume schemes. Adv Appl Math Mech 12:436–479. https://doi.org/10.4208/aamm.OA-2017-0243

115. Tang L, Song S, Zhang H (2020) High-order maximum-principle-preserving and positivity-preserving weighted compact nonlinear schemes for hyperbolic conservation laws. Appl Math Mech-Engl 41:173–192. https://doi.org/10.1007/s10483-020-2554-8

116. Zhang H, Xu C, Dong H (2021) An extended seventh-order compact nonlinear scheme with positivity-preserving property. Comput Fluids 229:105085. https://doi.org/10.1016/j.compfluid.2021.105085

117. Wong ML, Angel JB, Baradb MF et al (2021) A positivity-preserving high-order weighted compact nonlinear scheme for compressible gas-liquid flows. J Comput Phys 444:110569. https://doi.org/10.1016/j.jcp.2021.110569

118. Zhou Z, Ding J, Huang S et al (2023) A new type of weighted compact nonlinear scheme with minimum dispersion and adaptive dissipation for compressible flows. Comput Fluids 262:105934. https://doi.org/10.1016/j.compfluid.2023.105934

Publisher's Note